THE JOURNAL OF PHYSICAL CHEMISTRY C

Article

pubs.acs.org/JPCC

Chemistry, Impedance, and Morphology Evolution in Solid Electrolyte Interphase Films during Formation in Lithium Ion Batteries

Peng Lu,*[,†] Chen Li,[‡] Eric W. Schneider,[†] and Stephen J. Harris[§]

[†]Chemical & Materials Systems Lab, General Motors R&D Center, Warren, Michigan 48090, United States

[‡]Zee.Aero Inc., Mountain View, California 94043, United States

[§]Materials Science Division, Lawrence Berkeley National Lab, Berkeley, California 94720, United States

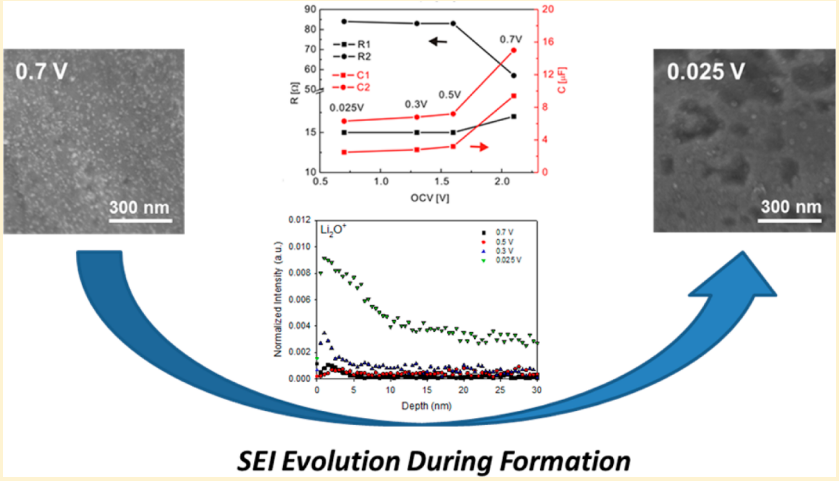

SEI Evolution During Formation

ABSTRACT: The solid electrolyte interphase (SEI) forms during the initial cycles in lithium ion batteries and evolves throughout the battery life. By protecting the electrode and passing lithium ions, the SEI plays an important role in the performance and degradation of lithium ion batteries. Identifying how the SEI forms and evolves during battery cycling helps us understand and mitigate battery degradation. In this work, we address the SEI chemical and electrochemical evolution during its formation process and provide a correlation between these properties. It is found that the SEI chemistry, not just its thickness, has a distinct influence on its impedance, which may ultimately impact the battery performance.

1. INTRODUCTION

Use of Li ion batteries in vehicles is a promising remedy to reduce the world's dependence on fossil fuels and ease global warming. However, significant challenges still exist to enable the large scale commercialization of this technology in plug-in hybrid electric vehicles (PHEVs) and full electric vehicles (EVs).[1−4] One of the crucial issues is to stabilize the electrolyte/electrode interface for long-term battery durability and safety.[5−7]

Solid electrolyte interphase (SEI) films play a critical role in the performance of Li ion batteries. They have two functions: to block electrons and to allow Li^+ ions to pass through. The deterioration of these functions is one of the most common causes of battery degradation.[8−16] If electrons are not blocked, the SEI films grow with continuous electrolyte decomposition on the electrode, consuming Li (and electrolyte) and reducing the battery capacity. If Li^+ ions cannot efficiently pass through the SEI, the cell impedance rises. Though great efforts have been made to improve the stability and performance of SEI films, we still have very little idea of just what SEI degradation means at the molecular level. For example, impedance can rise because the SEI becomes too thick or because its chemistry or morphology changes, but it has not been clear how to separate these effects. We know even less about molecular-scale causes for changes in the electrical conductivity of SEI films. Indeed, we know very little at the molecular level - even how a well-functioning SEI transports Li.

Previous work has been reported on surface electrochemical and mechanical changes during SEI formation. Zhang et al. measured the impedance of SEI films on graphite as a function of their formation voltage and reported that a loose and highly resistive SEI film formed above 0.25 V, whereas compact and more conductive SEI formed below 0.25 V accompanying graphite lithiation.[17] Tang and Newman used redox shuttles to characterize SEI-type passivating film formation on a glassy carbon electrode, and proposed that longer formation time resulted in lower SEI porosity.[11,18] In a recent work, they also found that SEI formed at lower potentials was more passivating and did not affect the system ohmic resistance.[19] On the

Received: November 11, 2013
Revised: December 16, 2013
Published: December 19, 2013

mechanical property side, Sheldon et al. reported the observation of irreversible compressive stress on graphite due to SEI formation, where most of the irreversible stress occurs from 0.75 to 0.25 V.[20] Consistent with previous findings, we find that SEI components evolve and contribute to the impedance differently, and the film porosity also changes during the formation process.

Inspired by the earlier work by Zhang et al.,[17] we focus on the SEI chemistry evolution at various voltages during formation, and we attempt to correlate SEI chemistry with its electrochemical and morphological properties. For the experiments described here, we use impedance spectroscopy, XPS, TOF-SIMS, and SEM to study the initial SEI formation process and report for the first time the relationships between SEI electrical, chemical, and morphological properties as a function of their formation voltage.

2. EXPERIMENTAL SECTION

2.1. Sample Preparation. SEI films were formed in LilCu coin half-cells, using a ~1 cm diameter copper foil (25 μm thickness) as the positive electrode, lithium metal of the same size as the negative electrode, and 1 M $LiPF_6$ in 1:1 ethylene carbonate (EC):dimethyl carbonate (DMC) as the electrolyte. We argued previously that SEI films grown below 0.8 V on Cu should be at least qualitatively similar to those grown at similar voltages on realistic electrode.[21] Because Cu does not insert Li, its use allows us to focus on the influence of voltage on SEI formation without any complications from the effects of voltage on Li insertion.[22] Four sets of SEI films were formed and studied, as described previously.[22] One cell was discharged galvanostatically at 2.5×10^{-5} A to 0.7 V and then held at this voltage until the current dropped to $<1 \times 10^{-6}$ A. This sample is denoted "SEI formed at 0.7 V". The second cell first went through the same procedure as the 0.7 V sample, but after the current dropped below 1 μA at 0.7 V, we discharged it at 2.5×10^{-5} A to 0.5 V and held it there until the current dropped below 1 μA to produce the "SEI formed at 0.5 V". Analogous procedures were employed to form SEI at 0.3 and 0.025 V. We note that this procedure may well produce a different material from an SEI formed by initially setting the voltage at a single value, e.g., 0.3 V, and allowing the current to decay. Our procedure allows us to determine how an SEI formed, for example, at 0.7 V evolves when the voltage is lowered to 0.5 V. Electrochemical impedance spectroscopy (EIS) measurements were performed after discharge at each voltage stage.

After SEI formation, the Cu foils with SEI were harvested from the coin cells in an Ar filled glovebox. Each sample was rinsed with 3 mL DMC for 15 s to remove the residual electrolyte, dried in Ar, and separated into two identical pieces. One piece was kept aside for analysis. The other piece was soaked in 1 M $LiBF_4$ EC:DMC 1:1 for 30 s, rinsed with 3 mL of DMC for 15 s, dried in Ar, and then transferred with the other samples for analyses.

Information about the SEI porous region properties can be obtained by soaking an SEI made with $LiPF_6$ salt in 1 M $LiBF_4$ EC:DMC 1:1 electrolyte. The $LiBF_4$ distribution in the SEI was analyzed by time-of-flight secondary ion mass spectrometer (TOF SIMS) depth profiling, where we assume that the $LiBF_4$ (identified by B^+ ion signal) in the electrolyte can penetrate the SEI only where it is porous (Scheme 1). If isotope labeled electrolyte is used, e.g., $^6LiBF_4$, this method can also be extended to measure Li transport behaviors in SEI by monitoring the ^6Li:^7Li isotope ratio.[22] For the TOF-SIMS analyses, SEI samples were transferred in Ar using a sealed apparatus, with no exposure to air. For the X-ray photoelectron spectroscopy (XPS) and scanning electron microscopy (SEM) analyses, samples were sealed in an Ar filled container prior to transfer, and exposure time to air was <30 s.

Scheme 1. Setup of Tracer Experiment for SEI Porosity Property Measurement[a]

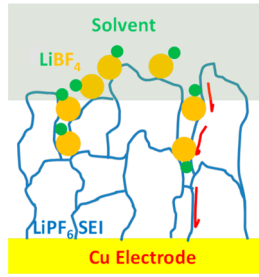

[a]Electrolyte can only penetrate SEI through the porous regions; thus the boron depth distribution provides information on thickness of the porous SEI region.

2.2. Instrumentation. The XPS analyses were conducted on a PHI Quantera XPS Scanning Microprobe (Physical Electronics, Chanhassen, MN) with a monochromated Al Kα source (1486.6 eV). The base pressure of the system was $<2.5 \times 10^{-7}$ Pa. A 1 kV Ar ion source was used for sputtering, and the sputter rate was ~2 nm/min calibrated on a 100 nm SiO_2 thin film. The analysis area was 1 mm × 1 mm, within a sputter area of 10 mm × 10 mm. A PHI TRIFT V nanoTOF spectrometer (Physical Electronics, Chanhassen, MN) was employed for the TOF SIMS analyses. The analysis chamber of the instrument was maintained at a pressure of less than 5×10^{-7} Pa during analysis. A 30 kV Au^+ ion source was used for both sputtering (~0.1 nm/s calibrated with 100 nm SiO_2) and analysis. The analysis area was 50 μm × 50 μm, within a sputter area of 200 μm × 200 μm. For SEI thickness calculation, a uniform sputter rate is assumed regardless of the SEI composition and porosity. SEM images were taken on a Carl Zeiss FIB-SEM CrossBeam Workstation (Carl Zeiss, Peabody, MA) at 5 mm working distance with 3 kV beam energy.

Electrochemical impedance spectroscopy (EIS) measurements for each coin cell were performed by using a Solartron FRA 1260 frequency response analyzer combined with a Solartron model 1287 electrochemical interface. The frequency range selected was between 100 kHz and 0.02 Hz. The potentiostatic signal amplitude was 5 mV. All impedance data shown here were fitted and simulated with ZView software (Scribner Associates, Southern Pines, NC).

3. RESULTS AND DISCUSSION

3.1. SEI Impedance and Thickness Evolution. After SEI formation, EIS (Figure 1a) were measured for the LilCu coin cells discharged to 0.7, 0.5, 0.3, and 0.025 V, whose open circuit voltages were 2.1, 1.6, 1.3, and 0.7 V, respectively. Due to the absence of intercalation materials in this system, the major response of the impedance is exclusively related to Li ion transport. All the spectra consist of a depressed semicircle and a sloping line. The equivalent circuit shown in the inset of Figure 1a is tentatively used to fit the impedance spectra. In the absence of active materials, the common features corresponding to charge transfer and solid-state diffusion are not observed in the impedance spectra. Thus the semicircles found at high

dx.doi.org/10.1021/jp4111019 | J. Phys. Chem. C 2014, 118, 896−903

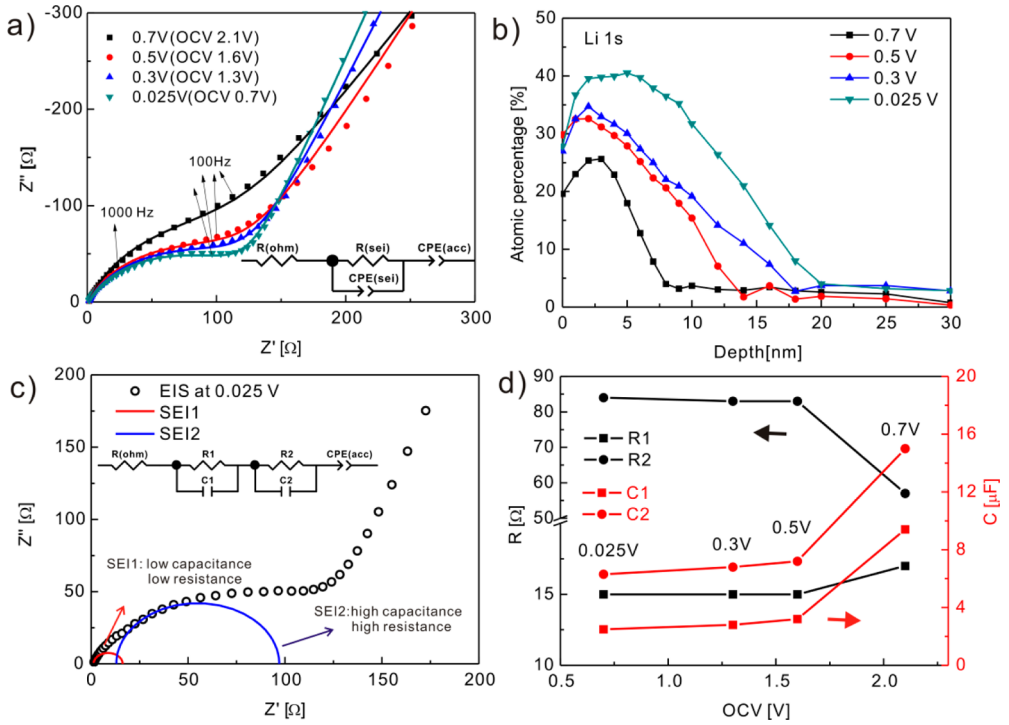

Figure 1. (a) Impedance spectra, (b) Li1s XPS depth profile (adapted with permission from our previous paper for discussion purpose; copyright American Chemical Society),[21] (c) impedance spectra fitted with two SEI layer components, and (d) fitted resistance and capacitance values over the voltage range of SEI formed at various voltages during the first half-cycle.

frequency region (10^3–10^4 Hz) are attributed exclusively to the SEI layer on both electrodes. In this case, ionic transport is blocked at the SEI/Cu interface. Thus a slopping line at lower frequency region represents a charge accumulation on the current collector in which the system shows a purely capacitive behavior. Similar characteristics have been discussed in the EIS measurement of SEI formed on other metals in three-electrode configurations.[23,24] To obtain a better fit for those depressed semicircles, the capacitor is replaced by constant phase elements (CPE). The depression of the semicircle, which indicates the nonideal behavior of the capacitor, has been attributed to porous microstructures and nonuniformity of electrode surfaces.[8,9,25,26] The resistances obtained from the fit are 81, 109, 118, and 118 Ω for SEI formed at 0.7, 0.5, 0.3, and 0.025 V, respectively.

In our recent review paper, we briefly mentioned that SEI thickness increased and morphology changed during SEI growth on Cu.[21] Here we report further study and in depth discussion on the correlation between SEI thickness and impedance. The SEI thicknesses on the copper surface are estimated from the presence of Li-containing components in the SEI. In Figure 1b, the Li1s XPS depth profiles show the depth distribution of Li-containing species that are identified in the SEI (e.g., LiF, Li_2CO_3, Li_2O, $ROCO_2Li$, etc.).[9,27] Because the SEI/Cu interface is not perfectly sharp, we arbitrarily define the interface location to be at half of the peak Li atomic percentage. In this case, the thicknesses of the SEI films formed at 0.7, 0.5, 0.3, and 0.025 V are 6, 9, 10, and 14 nm, respectively. Alternatively, the interface can also be defined in other ways, e.g., the Li1s at 5%, where the thickness of the SEI films formed at 0.7, 0.5, 0.3, and 0.025 V are 7, 12, 17, and 20 nm, respectively. Interestingly, no matter how the SEI thickness is defined, the resistance per unit thickness (Ω/nm) decreases as the SEI thickness increases at lower voltage (Table 1).

Table 1. Unit Thickness Resistance for SEI Formed at Various Voltages[a]

voltage (V)	SEI resistance	thickness (nm) (50% Li1s)	Ω/nm (50%)	thickness (nm) (5% Li1s)	Ω/nm (5%)
0.7	81	6	13.5	7	11.5
0.5	109	9	12.1	12	9.1
0.3	118	10	11.8	17	6.9
0.025	118	14	8.4	20	5.9

[a]SEI/Cu interface was defined at 50% of the Li1s peak intensity (50%) or 5% Li1s atomic percentage (5%).

The decreasing unit thickness resistance demonstrates that factors other than SEI thickness, such as varying chemical composition, can also account for the impedance variation during SEI evolution.

On the basis of these observations, one scenario of SEI layer growth can be proposed as follows. Initial SEI formation at higher voltages mainly consists of the growth of a loose and highly resistive layer (e.g., organic polymer); the total thickness of the SEI increases as the cell potential decreases, and simultaneously the SEI layer is transformed to more compact and relatively conductive component (e.g., inorganic salts). This proposal will be further elaborated and supported in the following discussions.

To further understand SEI evolution at different potentials, we attempt another EIS fitting strategy. The depression of the semicircles might also be due to a partial superimposition of two or even multiple semicircles, which actually results from a multiple layered structures of SEI.[22,28] An example is demonstrated in Figure 1c, where two SEI layer components with different capacitance and resistance characteristics are included in the fitting. The inset of Figure 1c shows the corresponding equivalent circuit, including two RC modules in series.

dx.doi.org/10.1021/jp4111019 | J. Phys. Chem. C 2014, 118, 896–903

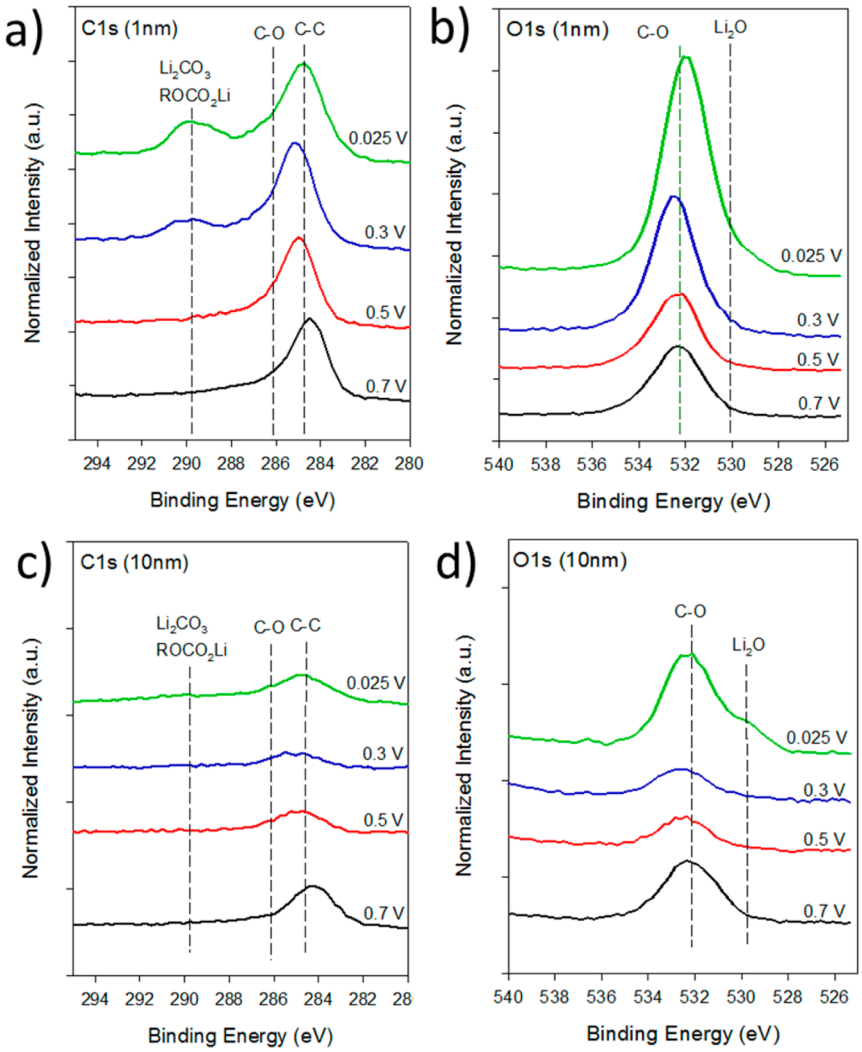

Figure 2. XPS spectra of SEI formed at different voltages: (a) C1s at 1 nm below surface; (b) O1s at 1 nm below surface; (c) C1s at 10 nm below surface; (d) O1s at 10 nm below surface. The absolute intensities of C1s and O1s spectra at 10 nm were much lower compared to the 1 nm intensities and have been scaled up for comparison purpose.

It should be noted that a real capacitor was used here. Here, we make some reasonable assumptions to correlate the EIS behaviors to SEI structural and chemical properties: Compared with a similar compact layer, a porous layer is likely to have higher capacitance; also organic species are generally less conductive than inorganic salts.

The resistance and capacitance values obtained from this fit are plotted in Figure 1d. From the fitting based on this two-layer structure of SEI, we summarize (1) the high frequency components (SEI 1) with low capacitance are always less resistive, which suggests that the compact layer may be more of inorganic nature; (2) with decreasing cell potential, both sorts of capacitances monotonically decrease, indicating a decrease of porosity of the SEI (i.e., a more compact structure was being formed); and (3) because the SEI thickness keeps increasing with decreasing cell potential, the SEI composition must evolve to less resistive components, given that the total resistance hardly changed below 0.5 V.

Although the choice of fitting model is relatively arbitrary, the two different models point to quite similar scenarios for the growth of the SEI layer. Our original proposal still holds well: SEI formation at higher voltages consists of the growth of a loose and highly resistive layer (likely organic carbonaceous species and Li organic polymer); at lower cell potential, the total thickness of the SEI layer increases and simultaneously the SEI layer is transformed to compact and relatively conductive components (e.g., inorganic salts).[17,29] This proposal will be further supported by additional chemical analyses data in the following discussions.

3.2. SEI Composition Evolution. A number of chemical reactions participate in the SEI formation process, and our data suggest that the dominant reactions at each voltage are different. Generally, the reactions that have been postulated or found in quantum mechanical calculations involve electrolyte solvent and salt reduction, with no reference to any reactions at the surface.[7,9,30,31] These reactions generate both organic (e.g., polymers) and inorganic products (e.g., Li_2CO_3, Li_2O, LiF, etc.). Ethylene carbonate may partially polymerize through surface assisted disproportion reactions and form polymer species in the SEI,[8] or it may also form ethylene glycol in a two-electron process and eventually become Li_2CO_3.[32] Because it is not our goal to elucidate the detailed reaction mechanisms in this study, only some generally proposed reactions in a $LiPF_6$ salt ethylene carbonate (EC) dimethyl carbonate (DMC) system are listed to show the common components of the SEI

dx.doi.org/10.1021/jp4111019 | J. Phys. Chem. C 2014, 118, 896−903

(eqs 1−6). We expect that each of these products contributes differently to the SEI impedance.

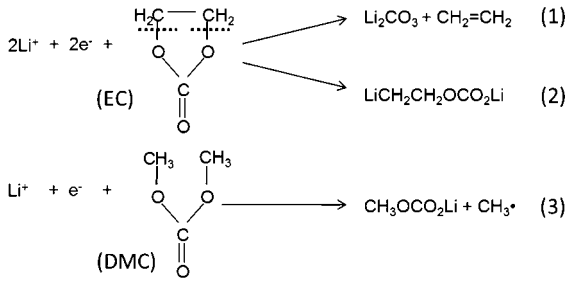

$$Li^+ + e^- + \text{Trace}\, H_2O \rightarrow LiOH + {}^1/_2\, H_2 \quad (4)$$

$$LiOH + e^- + Li^+ \rightarrow Li_2O + {}^1/_2\, H_2 \quad (5)$$

$$LiPF_6 \leftrightarrow LiF + PF_5 \xrightarrow{Li^+ + e^-} LiF + Li_xPF_y \quad (6)$$

The SEI composition evolution is studied with XPS and TOF-SIMS. The SEI films formed at various voltages are compared both near the electrolyte/SEI interface (noted as "1 nm", Figure 2a,b) and near the SEI/Cu interface (noted as "10 nm", Figure 2c,d), after removal of defined amount of SEI with Ar sputtering. Near the electrolyte/SEI interface (1 nm), only a broad peak at 284.5 eV (sp^2 C−C bonds) is observed in the XPS C1s spectra for SEI formed at 0.7 and 0.5 V (Figure 2a). C−O bonds are also identified by the presence of weak C1s peaks at 286.0 eV and O1s peaks at 532.2 eV (Figure 2a,b). The observation of such C−C and C−O features indicates that organic carbonaceous species start to form at the high voltage stage of SEI growth. In the later stages, for SEI films formed at 0.3 V and below, new C1s peaks at 290.0 eV emerge, indicating the formation of lithium carbonates and lithium alkyl carbonates. At 0.025 V, the C1s shoulder peak at 289.0 eV indicates a small amount of oxalate O−C−O formation at low voltages. This could be due to the formation of CO_2 and conversion to oxalate during the reduction process (Figure 2a).[33,34] Li_2O also forms at low voltages, because the weak O1s shoulder peak at 530.1 V is only visible at 0.025 V (Figure 2b).

At 10 nm below the SEI surface, C1s peaks at 290.0 eV are not observed in any of the SEI films; thus, Li_2CO_3 or $ROCO_2Li$ are not present at this depth (Figure 2c). Li_2O is only observed in the SEI formed at 0.025 V (Figure 2d), which is consistent with the 1 nm results. Notably, at this voltage, the ratio of the Li_2O O1s peak (530.1 eV) to the C−O peak (532.2 eV) at 10 nm is significantly higher than that ratio at 1 nm, indicating that Li_2O constitutes a larger portion of the SEI at 10 nm depth.

TOF SIMS depth profiles also support the observed SEI composition evolution. In Figure 3a, CH_3^+ ions are from the fragmentation of organic species with alkyl chains. These ions are observed in the 0.7 and 0.5 V SEI films, indicating that organic species start to form at high voltage stages. For SEI films formed at 0.3 and 0.025 V, CH_3^+ ions appear in much lower intensities. One scenario for the decreasing trend in organic species at low voltages can be the conversion to inorganic species like Li_2O, which is also supported by the change in Li_2O^+ ion profiles below. Notably, the CH_3^+ signals are still observed at low intensity even at 30 nm. These are artifacts due to the surface roughness of the substrate which results in trace amount of SEI residuals after sputtering.

Li_2O, Li_2CO_3, $ROCO_2Li$, and other carbonate-like species all generate Li_2O^+ fragmentation ions during TOF SIMS analyses.

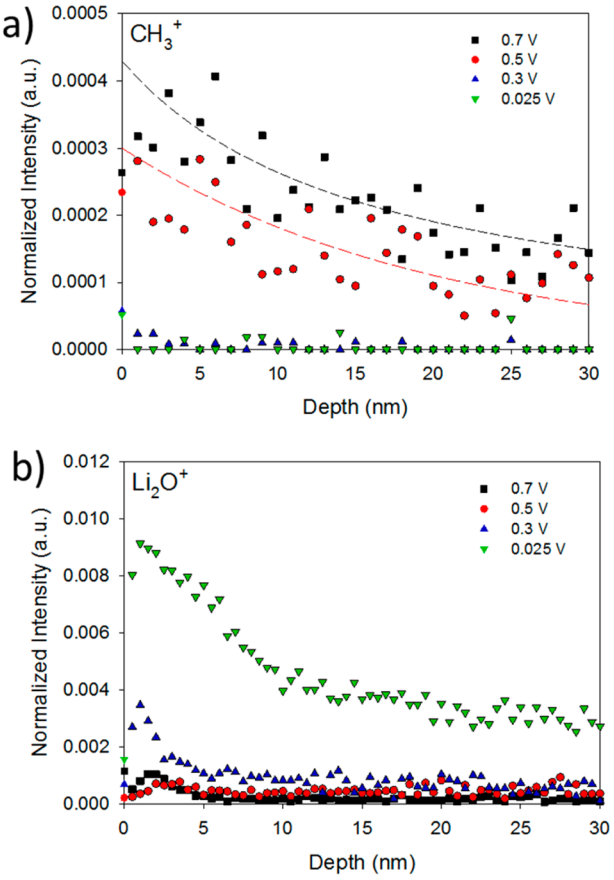

Figure 3. TOF SIMS depth profiles of SEI formed at different voltages: (a) CH_3^+; (b) Li_2O^+ fragmentation ions. Li_2O^+ and CH_3^+ intensities were normalized to total ion counts. The dashed lines are drawn to guide the eyes.

Within the top 5 nm, the SEI films formed at 0.3 and 0.025 V show significantly higher Li_2O^+ signals than the SEI films formed at 0.7 and 0.5 V, because lithium carbonates and lithium alkyl carbonates form only at lower voltages (Figure 3b). Beyond 10 nm, Li_2O^+ profiles from 0.7, 0.5, and 0.3 V SEI films all approach near zero baselines, whereas Li_2O^+ is still observed in the SEI formed at 0.025 V. Because Li_2O forms at 0.025 V (Figure 2), the Li_2O^+ signal should arise from $ROCO_2Li$ and carbonates for SEIs formed at 0.7, 0.5, and 0.3 V, in contrast to from Li_2CO_3 and Li_2O for SEI formed at 0.025 V. The Li_2O^+ profiles further confirm the XPS finding that Li_2CO_3 or $ROCO_2Li$ does not exist at 10 nm and Li_2O is a major inorganic component of the 0.025 V SEI film beyond 10 nm.

In summary, for the SEI studied, the organic components in the SEI form at the highest voltages, carbonates and/or alkyl carbonates then form at below 0.5 V, and lithium oxide forms last, at voltages lower than 0.3 V. Consistent with generally accepted SEI models,[6,25,27] organic species are mostly present near the electrolyte/SEI interface, whereas Li_2O is mainly observed near the SEI/Cu interface. Interestingly, some inorganic species, such as Li_2CO_3 and/or $ROCO_2Li$, are mostly present near the electrolyte interface. This suggests that the "inorganic" and "organic" categories may be too simple to describe the two-layer structure of SEI, although in this study, we found that such categories are still suitable in terms of discussing the thickness and composition evolution in different voltages. Combined with the impedance data, it appears that the organic components formed at high voltage (contributing

dx.doi.org/10.1021/jp4111019 | J. Phys. Chem. C 2014, 118, 896−903

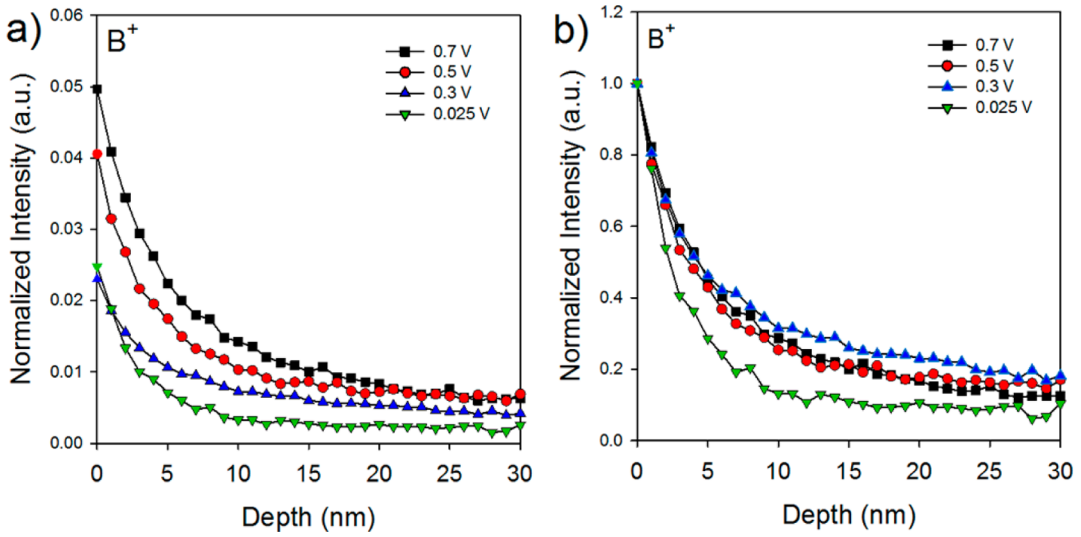

Figure 4. Tracer measurements for SEI nanoporous structure (porous region thickness). TOF SIMS depth profile of tracer B^+ ions in SEI formed at different voltages: (a) B^+ ions intensities were normalized to the total ion intensities; (b) the B^+ depth profile starting points (electrolyte/SEI interface) were normalized to unit value (1) to show clear trends (adapted with permission from our previous paper for discussion purpose; copyright American Chemical Society).[21]

to the low frequency impedance) are relatively less conductive, and the inorganic components formed below 0.5 V (contributing to the high frequency impedance) are more conductive.

3.3. SEI Nanoporous Structure Evolution. Our ability to quantitatively characterize the nanoporous nature of SEI has been described previously.[21,22] Here, we discuss this novel technique and SEI porosity changes during formation in more details. Using our electrolyte tracer technique, an approximation to the SEI porous region thickness can be obtained. Two assumptions are made to interpret the depth profile data. First, the electrolyte salt ($LiBF_4$) follows the solvent through porous regions in the SEI but without reacting. Thus the boron (B^+) depth profile reflects the SEI nanoporosity properties (Scheme 1). Second, the boron (B^+) signals are from the residual $LiBF_4$ deposited in the pores of the SEI, in an amount proportional to the surface areas of the pores. Thus the boron (B^+) signal intensity semiqualitatively reflects the degree of porosity in the SEI.

The B^+ depth profiles indicate that the SEI porosity properties changes significantly as a function of SEI formation voltage (Figure 4). More B^+ ions are observed from SEI formed at higher voltage, both at the electrolyte/SEI interface and throughout the SEI (Figure 4a). This shows that in general SEI formed at high voltages (e.g., 0.7 V) is more porous than SEI formed at low voltages (e.g., 0.025 V). Because organic products form at high voltage and inorganic species form at low voltage (Figures 2 and 3), this porosity property evolution also suggests that organic products are more porous than the inorganic products represented by Li_2CO_3, Li_2O, etc.

The B^+ intensities are also normalized to unit value (1) at the electrolyte/SEI interface to better show the porous region thickness in the SEI (Figure 4b). In the SEI films formed above 0.025 V, B^+ ions are observed all the way through the SEI thickness, indicating that these SEI films are porous at all depths. Notably, 0.3 V SEI consists of fewer organic species and more carbonates than 0.7 and 0.5 V SEI (Figure 3), and it is still porous. This indicates that the formation of carbonates reduces SEI porosity (Figure 4a), but Li_2CO_3 has to convert to

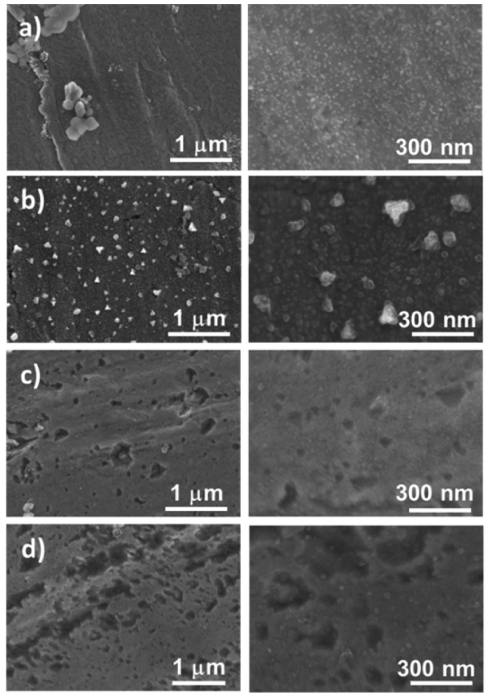

Figure 5. SEM images of SEI formed at (a) 0.7 V, (b) 0.5 V, (c) 0.3 V, and (d) 0.025 V (adapted with permission from our previous paper for discussion purpose; copyright American Chemical Society).[21] Each set of images were shown in two magnification scales: images on the left are at ×30 k and images on the right are at ×100 k.

even denser species (e.g., Li_2O) to stop electrolyte penetration (Figure 4b). In the 0.025 V SEI, B^+ ions penetrate only ~10 nm, which is about halfway through its thickness. This demonstrates the presence of a dense (nonporous) layer that prevents electrolyte solution from penetrating deeper than ~10 nm into the SEI. Considering the XPS and TOF SIMS results, that Li_2O is the major component of the SEI layer formed at 0.025 V at 10 nm (Figures 2d and 3b), a dense Li_2O layer is likely responsible for the drop in porosity suggested by

dx.doi.org/10.1021/jp4111019 | J. Phys. Chem. C 2014, 118, 896−903

the change in the B^+ depth profile. The correlation between SEI compositions and porosity properties further supports our proposal that porous organic species convert to dense inorganic species as voltage decreases.

3.3. SEI Morphology Evolution. As described in our previous paper,[21] SEI films formed at different voltages also show a clear trend of morphology evolution (Figure 5). At higher (0.7 and 0.5 V) voltages, the substrate is covered with a uniform layer embedded with scattered nanometer size crystallites, which are confirmed to be LiF by EDX (Figure 5a,b). The LiF crystallites grow larger as the voltage reduces to 0.5 V, but at 0.3 V and below, discrete LiF crystallites are no longer observed on the surface (Figure 5b,c). Instead, the surface film shows holes or dents of micrometer sizes at 0.3 V, which we take as evidence for gas formation inside the SEI, as predicted by reactions 1, 4, and 5 above. At 25 mV the surface becomes rougher with more and larger holes, indicating that the gas formation reactions continue to occur at low voltage (Figure 5d). To the extent that these holes penetrate to the surface, new SEI would have grown. We cannot speculate about whether gas forming reactions also occur at higher voltages, because the highly porous films might not fracture in the presence of gas formation. Although not visible in some of the SEM images, LiF is observed in all the SEI films studied by TOF SIMS (Figure 6). The reason that discrete LiF crystallites are not observed below 0.5 V might be that the crystallites are covered by the surface organic layer or that the crystallites are too small to see.

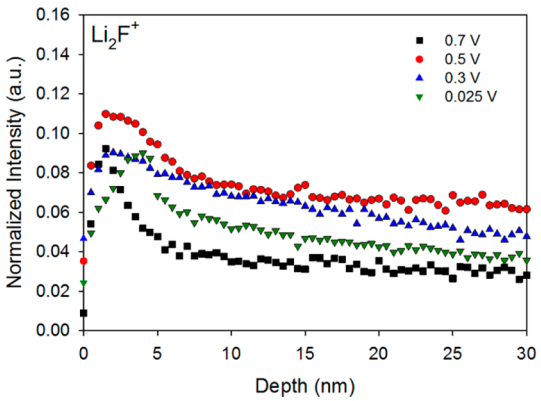

Figure 6. TOF SIMS depth profile of Li_2F^+ in SEI formed at various voltages. Li_2F^+ was a fragmentation ion from LiF, and the intensities were normalized to total ion counts.

4. CONCLUSIONS

Our results suggest some new ways of thinking about SEI formation and growth.

1. The fact that the impedance per unit thickness drops with voltage demonstrates that the SEI thickness is not the only factor contributing to its impedance. This result is consistent with that of Zhang et al., who grew SEI films at constant voltages on graphite particles and found, in his case, that the impedance actually fell as the voltage was lowered.[17] Thus, chemical composition and/or morphology must also play important roles in determining impedance. Though this should not seem surprising, the assumption that impedance is proportional to the SEI thickness is common[35] and has been used to rationalize the $t^{1/2}$ dependence of fade. There can be little doubt that as electrodes age and the SEI thickens, impedance increases. Our point here, however, is that the relationship between SEI thickness and impedance is complex.
2. In the generally accepted SEI model, the "inorganic" and "organic" categories may need to be elaborated, and a more chemically specific definition may be required when the two-layer structure of the SEI is described. In the SEI we studied here, organic species are mostly present in the outer layer (close to the electrolyte), and Li_2O is mainly observed in the inner part (close to the electrode) in the SEI. Interestingly, some inorganic species, such as Li_2CO_3 and/or $ROCO_2Li$, are also mostly present near the electrolyte/SEI interface (outer part). However, in terms of discussing the thickness and composition evolution at different voltages, we find that such categories are still suitable in this study.
3. The organic reduction products that are mostly seen in the outer part of the SEI (closer to the electrolyte) form at higher voltages and are relatively less conductive. That is, the material that becomes the outer layer actually forms first. The inorganic components, such as Li_2CO_3 and Li_2O, form only after the voltage falls to 0.3 V and below. Compared with organic species, the inorganic SEI components are more conductive but less capacitive, resulting in a decrease in impedance per unit thickness.
4. Our results suggest that the inorganic (Li_2O) layer forms by conversion of some of the organic outer layer, because the porous (largely organic) layer is actually thinner at 25 mV than at 0.3 V and above (Figures 3 and 4b). The dense Li_2O layer prevents electrolyte from reaching the electrode and provides better protection to the electrode. It is also reasonable that such conversion (reduction) should occur closest to the negative electrode.

In this work, the microscale SEI chemistry, impedance, and morphology evolution at different voltages have been revealed. It is found that the SEI chemistry, not just its thickness, has a distinct influence on its impedance, which may ultimately impact the battery performance. Understanding SEI formation and evolution under various conditions, as well as designing SEI with specific properties, will be the subjects of future work.

AUTHOR INFORMATION

Corresponding Author

*P. Lu: e-mail, peng.lu@gm.com; ph, 586-929-3075; fax, 586-986-1932.

Notes

The authors declare no competing financial interest.

ACKNOWLEDGMENTS

The authors acknowledge Curt Wong from GM R&D for his help with the SEM characterization. We also thank Michael Balogh, Nicholas Irish, Richard Waldo, Yue Qi, and Xingcheng Xiao from GM R&D for useful discussions.

REFERENCES

(1) Goodenough, J. B.; Kim, Y. Challenges for Rechargeable Li Batteries. *Chem. Mater.* **2010**, *22*, 587−603.

(2) Bruce, P. G. Energy Storage Beyond the Horizon: Rechargeable Lithium Batteries. *Solid State Ionics* **2008**, *179*, 752−760.

(3) Thackeray, M. M.; Wolverton, C.; Isaacs, E. D. Electrical Energy Storage for Transportation — Approaching the Limits of, and Going

Beyond, Lithium-Ion Batteries. *Energy Environ. Sci.* **2012**, *5*, 7854−7863.
(4) Armand, M.; Tarascon, J.-M. Building Better Batteries. *Nature* **2008**, *451*, 652−657.
(5) Vetter, J.; Nováak, P.; Wagner, M. R.; Veit, C.; M̈oller, K.-C.; Besenhard, J. O.; Winter, M.; Wohlfahrt-Mehrens, M.; Vogler, C.; Hammouche, A. Ageing Mechanisms in Lithium-Ion Batteries. *J. Power Sources* **2005**, *147*, 269−281.
(6) Winter, M. The Solid Electrolyte Interphase - the Most Important and the Least Understood Solid Electrolyte in Rechargeable Li Batteries. *Z. Phys. Chem.* **2009**, *223*, 1395−1406.
(7) Xu, K.; Cresce, A. v. Interfacing Electrolytes with Electrodes in Li Ion Batteries. *J. Mater. Chem.* **2011**, *21*, 9846−9864.
(8) Aurbach, D.; Markovsky, B.; Weissman, I.; Levia, E.; Ein-Eli, Y. On the Correlation between Surface Chemistry and Performance of Graphite Negative Electrodes for Li Ion Batteries. *Electrochim. Acta* **1999**, *45*, 67−86.
(9) Aurbach, D. Review of Selected Electrode−Solution Interactions Which Determine the Performance of Li and Li Ion Batteries. *J. Power Sources* **2000**, *89*, 206−218.
(10) Edstrom, K.; Herstedt, M.; Abraham, D. P. A New Look at the Solid Electrolyte Interphase on Graphite Anodes in Li-Ion Batteries. *J. Power Sources* **2006**, *153*, 380−384.
(11) Tang, M.; Newman, J. Electrochemical Characterization of SEI-Type Passivating Films Using Redox Shuttles. *J. Electrochem. Soc.* **2011**, *158*, A530−A536.
(12) Smith, A. J.; Burns, J. C.; Zhao, X.; Xiong, D.; Dahn, J. R. A High Precision Coulometry Study of the Sei Growth in Li/Graphite Cells. *J. Electrochem. Soc.* **2001**, *158*, A447−A452.
(13) Xiao, X.; Lu, P.; Ahn, D. Ultrathin Multifunctional Oxide Coatings for Lithium Ion Batteries. *Adv. Mater.* **2011**, *23*, 3911−3915.
(14) Jung, Y. S.; Lu, P.; Cavanagh, A. S.; Ban, C.; Kim, G.-H.; Lee, S.-H.; George, S. M.; Harris, S. J.; Dillon, A. C. Unexpected Improved Performance of Ald Coated $LiCoO_2$/Graphite Li-Ion Batteries. *Adv. Energy Mater.* **2013**, *3*, 213−219.
(15) Shearing, P. R.; Howard, L. E.; Jørgensen, P. S.; Brandon, N. P.; Harris, S. J. Characterization of the 3-Dimensional Microstructure of a Graphite Negative Electrode from a Li-Ion Battery. *Electrochem. Commun.* **2010**, *12*, 374−377.
(16) Deshpande, R.; Verbrugge, M.; Cheng, Y. T.; Wang, J.; Liu, P. Battery Cycle Life Prediction with Coupled Chemical Degradation and Fatigue Mechanics. *J. Electrochem. Soc.* **2012**, *159*, A1730−A1738.
(17) Zhang, S.; Ding, M. S.; Xu, K.; Allen, J.; Jow, T. R. Understanding Solid Electrolyte Interface Film Formation on Graphite Electrodes. *Electrochem. Solid-State Lett.* **2001**, *4*, A206−A208.
(18) Tang, M.; Newman, J. Transient Characterization of Solid-Electrolyte-Interphase Using Ferrocene. *J. Electrochem. Soc.* **2012**, *159*, A281−A289.
(19) Tang, M.; Lu, S.; Newman, J. Experimental and Theoretical Investigation of Solid-Electrolyte-Interphase Formation Mechanisms on Glassy Carbon. *J. Electrochem. Soc.* **2012**, *159*, A1775−A1785.
(20) Mukhopadhyay, A.; Tokranov, A.; Xiao, X.; Sheldon, B. W. Stress Development Due to Surface Processes in Graphite Electrodes for Li-Ion Batteries: A First Report. *Electrochim. Acta* **2012**, *66*, 28−37.
(21) Harris, S. J.; Lu, P. Effects of Inhomogeneities—Nanoscale to Mesoscale—on the Durability of Li-Ion Batteries. *J. Phys. Chem. C* **2013**, *117*, 6481−6492.
(22) Lu, P.; Harris, S. J. Lithium Transport within the Solid Electrolyte Interphase. *Electrochem. Commun.* **2011**, *13*, 1035−1037.
(23) Zaban, A.; Aurbach, D. Impedance Spectroscopy of Lithium and Nickel Electrodes in Propylene Carbonate Solutions of Different Lithium Salts: A Comparative Study. *J. Power Sources* **1995**, *54*, 289−295.
(24) Schranzhofer, H.; Bugajski, J.; Santner, H. J.; Korepp, C.; Möller, K.-C.; Besenhard, J. O.; Winter, M.; Sitte, W. Electrochemical Impedance Spectroscopy Study of the SEI Formation on Graphite and Metal Electrodes. *J. Power Sources* **2006**, *153*, 391−395.
(25) Peled, E.; Golodnitsky, D.; Ardel, G. Advanced Model for Solid Electrolyte Interphase Electrodes in Liquid and Polymer Electrolytes. *J. Electrochem. Soc.* **1997**, *144*, L208−L210.
(26) Aurbach, D.; Markovsky, B.; Shechter, A.; Ein-Eli, Y.; Cohen, H. A Comparative Study of Synthetic Graphite and Li Electrodes in Electrolyte Solutions Based on Ethylene Carbonate-Dimethyl Carbonate Mixtures. *J. Electrochem. Soc.* **1996**, *143*, 3809−3820.
(27) Verma, P.; Maire, P.; Novák, P. A Review of the Features and Analyses of the Solid Electrolyte Interphase in Li-Ion Batteries. *Electrochim. Acta* **2010**, *55*, 6332−6341.
(28) Shi, S.; Lu, P.; Liu, Z.; Qi, Y.; Louis G. Hector, J.; Li, H.; Harris, S. J. Direct Calculation of Li-Ion Transport in the Solid Electrolyte Interphase. *J. Am. Chem. Soc.* **2012**, *134*, 15476−15487.
(29) Zhang, S.; Xu, K.; Jow, T. R. EIS Study on the Formation of Solid Electrolyte Interface in Li-Ion Battery. *Electrochim. Acta* **2006**, *51*, 1636−1640.
(30) Tarascon, J.-M.; Armand, M. Issues and Challenges Facing Rechargeable Lithium Batteries. *Nature* **2001**, *414*, 359−367.
(31) Laruelle, S.; Pilard, S.; Guenot, P.; Grugeon, S.; Tarascon, J. M. Identification of Li-Based Electrolyte Degradation Products through DEI and ESI High-Resolution Mass Spectrometry. *J. Electrochem. Soc.* **2004**, *151*, A1202.
(32) Leung, K. Two-Electron Reduction of Ethylene Carbonate: A Quantum Chemistry Re-Examination of Mechanisms. *Chem. Phys. Lett.* **2013**, *568*−*569*, 1−8.
(33) Dedryvère, R.; Laruelle, S.; Grugeon, S.; Gireaud, L.; Tarascon, J. M.; Gonbeau, D. XPS Identification of the Organic and Inorganic Components of the Electrode/Electrolyte Interface Formed on a Metallic Cathode. *Journal of The Electrochemical Society* **2005**, *152*, A689.
(34) Xu, K. Nonaqueous Liquid Electrolytes for Lithium-Based Rechargeable Batteries. *Chem. Rev.* **2004**, *104*, 4303−4418.
(35) Broussely, M.; Herreyre, S.; Biensan, P.; Kasztejna, P.; Nechev, K.; Staniewicz, R. J. Aging Mechanism in Li Ion Cells and Calendar Life Predictions. *J. Power Sources* **2001**, *97*−*98*, 13−21.